ACS OMEGA

http://pubs.acs.org/journal/acsodf

Article

Reaction of Ta_3^- Clusters with Molecular Nitrogen: A Mechanism Investigation

Xiaoli Sun* and Xuri Huang*

Cite This: *ACS Omega* 2022, 7, 22682−22688

Read Online

ACCESS | Metrics & More | Article Recommendations | Supporting Information

ABSTRACT: Because of the inertness of molecular nitrogen, its practicable activation under mild conditions is a fundamental challenge. Ta_3^- is an exceptionally small cluster that reacts with N_2 at room temperature, leading finally to $Ta_3N_2^-$; $Ta_3N_2^-$ also could react with N_2 at room temperature, leading finally to $Ta_3N_4^-$, a product of interest in its own right because of its potential as a nitrogen fixation medium. The mechanisms of the Ta_3^-- and $Ta_3N_2^-$-mediated activation of the N≡N triple bond have been investigated. Our extensive computations elucidate mechanisms for the ready reactions, leading to stepwise cleavage of the N≡N bond. Initial isomeric N_2/Ta_3^- complexes, N≡N elongation, undergo a N≡N split over generally low barriers in a highly exothermic process. The nitrogen-atom or molecular exchange reactions found in the $Ta_3N_2^-/N_2$ system may be of paramount importance in both applied and fundamental studies.

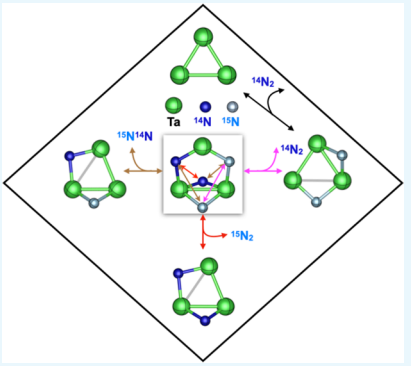

1. INTRODUCTION

The atmospheric abundance, accessibility, and nontoxicity of N_2 make it particularly desirable for us to construct N-containing compounds,[1−4] such as typical synthetic ammonia reaction.[5−9] However, the functionalization of N_2 represents a major challenge for modern chemistry due to its stability. The stability could be accounted for the lack of the dipole moment, the high bond dissociation energy (941 kJ mol^{-1}), high ionization energy (15.58 eV), the low proton and electron affinities (5.1 and −1.9 eV respectively),[6,10−12] as well as the very low lying, completely filled σ- and π-molecular orbitals and substantial energy gap between the highest occupied molecular orbital (−15.6 eV) and the lowest unoccupied molecular orbital (7.3 eV).

Vol'Pin and Shur were the first to study nitrogen fixation with transition-metal complexes.[13] Transition metals (M) could weaken or break the strong triple bond (N≡N) by donating electrons from d orbitals to empty antibonding π and σ orbitals of N_2 (Scheme 1a). In return, electron donation from fully filled π- and σ-orbitals of N_2 to vacant M orbitals could be found as well (Scheme 1b).[14−16] The former donation is vital in enabling N_2 binding and reduction, following which metal−nitrogen formed and strengthened. However, the latter donation is relatively small. By extension, the complete splitting of the N≡N by metal clusters is essentially governed by combining the two donations.[16,17]

Moreover, the M−N_2 binding mode strongly depends on the nature of the metal center. The different coordination modes generally show different orbital interaction modes and charge transfer and also different kinds of activation of the N≡N bond.[19,20] There are four possible coordination modes (Scheme 2): (1) end-on (η^1-N_2, M−M−N≡N, Scheme 2a), N_2 gets activated upon η^1-coordination to the first metal center, so the electron density in the antibonding orbitals in N_2 increases, rendering the coordinated molecule a better base for another metal center, (2) end-on bridging (Scheme 2b), μ-η^1-η^1-N_2, generally, M−M−N≡N and M−N≡N−M are more or less linear to allow for efficient orbital overlap. (3) Side-on mode (η^2-N_2, Scheme 2c) and μ-η^2-η^2-N_2 bridging coordination mode

Scheme 1. Orbital Interactions between N_2 and Transition Metal (M)

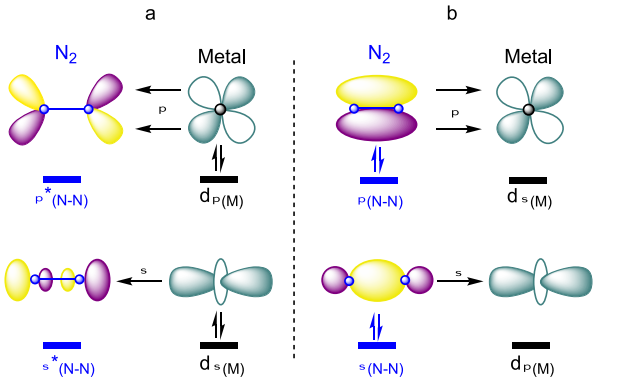

Received: April 6, 2022
Accepted: May 10, 2022
Published: June 21, 2022

Scheme 2. Possible Modes of N_2 Coordination to Transition Metal

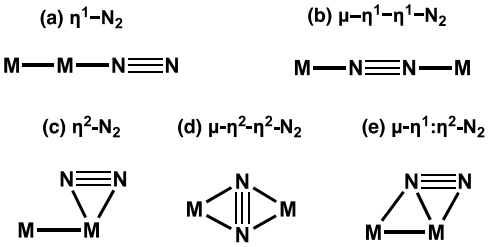

(Scheme 2d) is not as usual as the end-on one. Compared to end-on mode involving two M−N π-bonds, there is only one π-bond, while σ donation and backdonation (Scheme 1a,b) probably were not involved. Therefore, the end-on mode usually is energetically preferred than the side-on mode.[21] (4) Side-on-end-on (μ-η^1:η^2-N_2) (Scheme 2e), exhibiting a side-on coordination of N_2 to one metal center and an end-on coordination to the other.

Metal clusters have been found to be able to react with N_2.[22−31] However, most of the studied clusters can only adsorb N_2, and a few of them can split the N≡N under moderate conditions such as Sc, Ti, Gd, Co, Fe, and Ta clusters.[17,32−42] Among them, it was recognized that Ta clusters give outstanding performances to split the N≡N completely since the Ta−Ta center has enough reductivity to store electrons of N_2.[43,44]

As shown by the recent investigations, the extent of N≡N elongation varies with the model cluster size.[45] Larger clusters are favorable for N_2 adsorption. However, it does not necessarily have higher activity towards N_2 activation. Studies predicted that N_2 molecule activation is accessible at ambient temperature by small Ta_n^+ clusters (n = 2, 3, 4). The rate-limiting transition states is located at −55, −44, and −59 kJ mol^{-1} for Ta_2^+,[16] Ta_3^+, and Ta_4^+,[46] respectively, however it is located above the entrance asymptote for Ta_6^+.[35] Significantly, during N_2 activation by Ta_4^+ and Ta_6^+, the surface Ta−Ta−Ta acted as a protagonist, and the other Ta atoms were not directly involved or played only a minor role in N_2 cleavage. The Ta_3 moiety is the key structural unit of Ta series clusters and surfaces in N_2 cleavage. It is particularly important to study N_2 activation by Ta ternary clusters. Moreover, our studies indicated that an anionic system can give better kinetic activity and thermodynamic stability of the product than cationic and neutral ones.[47,48] V and Ta-nitride,[37,49] V and Ta-carbide,[36,50−52] and Co hydride[53] anion clusters are identified to be highly reactive toward N≡N bond cleavage by combining quantum chemistry calculations and experimental studies. Motivated by the vivid and splendid studies, we present detailed mechanisms of the first and second N_2 activation by anion cluster Ta_3^- at a molecular level, which probably would be taken as a model in the cluster and surface reactions.

2. COMPUTATIONAL DETAILS

All calculations were carried out by using the Gaussian 09 package.[54] The high quality of the triple-ζ def2-TZVP basis set was confirmed in previous, rather extensive studies.[55−57] For the Ta metal atoms, an effective core potential (ECP) is used for an approximate treatment of relativistic effects. We used the Becke-3-Lee−Yang−Parr (B3LYP) functional, which has already been successfully applied in the Ta_2^+/N_2 and Ta_2N^+/N_2 systems.[16,17] Furthermore, Armentrout and co-workers reported that B3LYP provides bond energies for MO^+ and MO_2^+ (M = Ta, W), which correspond very well to experimental data.[18]

Harmonic vibrational frequencies were computed to verify the nature of the stationary points. To corroborate the correct link between the minima and the transition states (TSs), intrinsic reaction coordinate[58−61] calculations were performed. Unscaled vibrational frequencies were used to calculate the zero-point energy contributions; thermal corrections to the enthalpy (ΔH) within the ideal-gas, rigid-rotor, harmonic-oscillator approximation at a temperature of 298 K and a pressure of 1 atm have been applied.

To obtain possible low-energy structures on the landscapes of the $\mathbf{Ta_3^-/N_2}$ and $\mathbf{Ta_3N_2^-/N_2}$ couples, the ABCluster[62] has been used to generate guess structures of $\mathbf{Ta_3N_2^-}$ and $\mathbf{Ta_3N_4^-}$ clusters. The def2-SVP basis set was adopted in the initial calculations, which produced more than 200 optimized structures. Subsequently, the lowest-lying isomers were re-optimized at the B3LYP/def2-TZVP level to obtain the global minimum structures of $\mathbf{Ta_3N_2^-}$ and $\mathbf{Ta_3N_4^-}$.

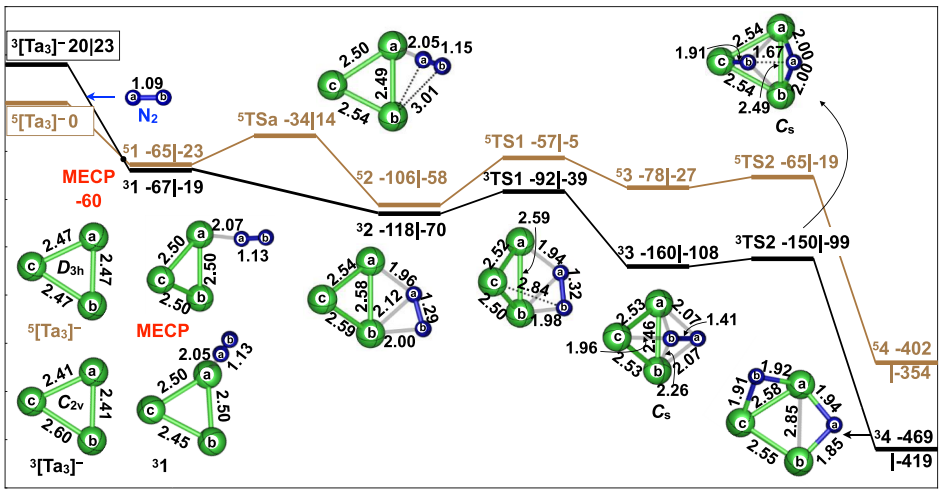

Figure 1. Simplified PES (ΔH_{298K} in kJ mol^{-1}) for Ta_3^-/N_2 coupling at the B3LYP/def2-TZVP + ECP level of theory. Key structures including selected geometric parameters are also provided. Bond lengths are given in angstrom and relative energies are given with respect to the entrance asymptote. ΔG (kJ mol^{-1}) is behind the vertical line.

https://doi.org/10.1021/acsomega.2c02138
ACS Omega 2022, 7, 22682−22688

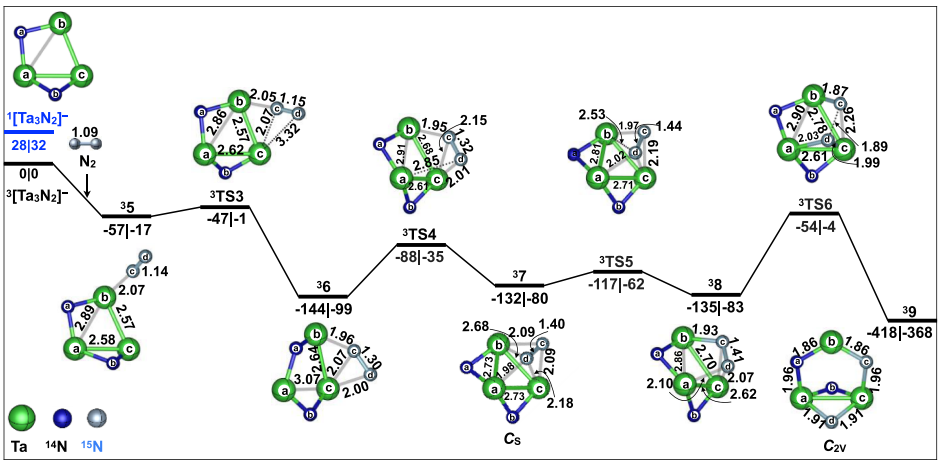

Figure 2. Simplified PES (ΔH_{298K} in kJ mol^{-1}) of $Ta_3N_2^-/N_2$ coupling at the B3LYP/def2-TZVP + ECP level of theory. Key structures including selected geometric parameters are also provided. Bond lengths are given in angstrom and relative energies are given with respect to the entrance asymptote. ΔG (kJ mol^{-1}) is behind the vertical line.

3. RESULTS AND DISCUSSION

3.1. Ta_3^- Mediates the N≡N Bond to Form $Ta_3N_2^-$. The optimal potential energy surface (PES) and structural parameters of key species for Ta_3^- mediates N≡N activation at B3LYP/def2-TZVP are shown in Figure 1. Three possible spin states, singlet, triplet, and quintet, are invested (Figure S1). The left superscript 1/3/5 is used to represent the singlet/triplet/quintet state (e.g., $^{1/3/5}$1). The ground state of Ta_3^- is a quintet, which is 20 and 29 kJ mol^{-1} lower than the triplet and singlet, respectively.

The Ta_3^-/N_2 coupling starts from either the quintet or triplet separated reactants, and it is subject to a two-state reactivity mechanistic scenario. The triplet/quintet PES crosses at the minimum energy crossing point (MECP,−60 kJ mol^{-1}), which could turn a spin flip from the quintet to the triplet surface and lead to obtaining the intermediate ^{3}1, releasing −67 kJ mol^{-1} of heat. The optimized structure indicates an end-on η^1-N_2 coordination mode with the distances of Ta^a−N^a = 2.05 Å and N^a−N^b = 1.15 Å. Subsequently, the triplet dominates the PES, so the triplet mechanism is mainly discussed below. Ta^b attacks N≡N further in a side-on manner to obtain a well-known combining end-on/side-on mode ^{3}2 (μ-η^1:η^2-N_2) releasing −118 kJ mol^{-1} energy. In ^{3}2, the end-on bond length between the terminal nitrogen atom (N^a) and Ta^a is 1.96 Å, and the side interaction between Ta^b and N^a−N^b forms Ta^b−N^a (2.12 Å) and Ta^b−N^b (2.00 Å) bonds. Compared with the separation reactant, the N≡N bond is weakened, and the bond length of the N≡N bond is elongated by 0.20 Å. Meanwhile, the Ta^a−Ta^b bond is elongated from 2.47 to 2.58 Å. Note that from ^{3}1 to ^{3}2, no barrier is encountered. However, in the Ta_4^+/N_2 system studied by Fries et al., this step requires merely an activation of 5 kJ mol^{-1}.[46]

The N≡N bond is elongated to 1.41 Å by the interaction of N^b with the third Ta atom (Ta^c) through the transition state ^{3}TS1 with an energy below the entrance asymptote of −92 kJ mol^{-1} generating ^{3}3 (−160 kJ mol^{-1}; C_s symmetry). N^b is changed from being interacted only with Ta^b in ^{3}2 to being interacted with the three Ta atoms. That is, the geometric structure is transferred from a η^2 to η^3 coordination, and this transformation is the rate-limiting step which is called the across edge-above surface (AEAS) mechanism by Fries et al. The prediction that AEAS operates significantly more likely on small clusters is confirmed.[46] Note that the rate-limiting transition state ^{3}TS1 in Ta_3^-/N_2 coupling has the lowest energy among those in Ta_2^+, Ta_4^+, and Ta_6^+/N_2 couplings.[16,35,46] Finally, N≡N is completely broken through the transition state ^{3}TS2 with a low energy barrier of 10 kJ mol^{-1}, generating the lowest energy intermediate ^{3}4 (−469 kJ mol^{-1}; C_s symmetry). In addition, there are other reaction paths for Ta_3^-/N_2 coupling (Figure S2), but they are disadvantageous on PES.

3.2. $Ta_3N_2^-/N_2$ Coupling. $Ta_3N_2^-$ (4 in Figure 1)/N_2 coupling is quite complicated (Figure S3). Only the optimal PES and structural parameters of key species are shown in Figure 2. The ground state of $Ta_3N_2^-$ is triplet, which is 32 and 67 kJ mol^{-1} lower than singlet and quintet, respectively (Figure S1). Moreover, the triplet species along the PES have more thermodynamic stability than the other two states, and there is no crossing point on the PES. Therefore, only the triplet state is studied.

First, N_2 approaches the $Ta_3N_2^-$ through the end-on mode (μ-η^1) to form ^{3}5 (−57 kJ mol^{-1}). Inspecting the geometric features of ^{3}5, the N^c−Ta^b bond length is 2.07 Å. Compared with the separated reactant, the N≡N bond is slightly weakened and the length is elongated by 0.05 Å. Then, N^c and N^d interact further with Ta^c in a side-on manner to obtain end-on/side-on mode ^{3}6 (μ-η^1:η^2-N_2), releasing −144 kJ mol^{-1} energy. The length of the N≡N bond in ^{3}6 is elongated by 0.16 Å than that of ^{3}5. The extension of the N≡N bond is similar to that in the Ta_3^-/N_2 coupling. At the same time, the three Ta atoms become detached and Ta and N become intimate in ^{3}6, for instance, the Ta^b−Ta^c bond is elongated to 2.64 Å, the end-bonded Ta^b−N^c bond length is 1.96 Å, and the side-bonded Ta^b−N^c and Ta^b−N^d bond lengths are 2.07 and 2.00 Å, respectively. The transition state ^{3}TS3 is located 10 kJ mol^{-1} above that of ^{3}5. However, in Ta_3^-/N_2, this step is no barrier.

The N≡N bond is elongated for a third time similar to AEAS. N^d interacts with the third Ta atom (Ta^a) through ^{3}TS4, which is located −88 kJ mol^{-1} below the entrance asymptote to generate ^{3}7 (−132 kJ mol^{-1}; C_s symmetry). In ^{3}7, the N≡N bond is elongated to 1.40 Å, which is 0.10 Å longer than that of ^{3}6. Subsequently, from ^{3}7, the N≡N bond could also be a cleavage finally through one transition state (^{3}TS17), generating ^{3}18. However, the energy barrier (−6 kJ mol^{-1} below the entrance) is much higher and ^{3}18 is not the lowest energy structure on the landscapes. Surprisingly, a lower energy channel was detected,

https://doi.org/10.1021/acsomega.2c02138
ACS Omega 2022, 7, 22682−22688

and it can lead to the lowest energy structure (^{3}9, −418 kJ mol^{-1}) on the landscapes, which is one step more than Ta_3^-/N_2 coupling. This path can be described in detail as follows. From ^{3}7 to ^{3}8, Ta and N become more intimate; for instance, the Ta^b-N^c bond is shortened from 2.09 to 1.93 Å, and Ta^c-N^d is shortened from 2.18 to 2.07 Å. Meanwhile, the Ta^b-Ta^c bond is elongated to 2.70 Å. In this process, the N≡N bond is only slightly elongated, from 1.40 to 1.41 Å, and only needs to pass through the transition state ^{3}TS5 with an energy of −117 kJ mol^{-1}. However, the energy of the transition state ^{3}TS6 (−54 kJ mol^{-1}) through which the N^c-N^d bond is completely destroyed is much higher than that of ^{3}TS2 (−150 kJ mol^{-1}) in the Ta_3^-/N_2 coupling. From the perspective of the activation energy barrier, the rate-determining transition state is ^{3}TS6.

Incidentally, if the remaining intermediate ^{3}9 is taken as the start of the PES, $Ta_3{}^{14}N^{15}N^-$ + $^{14}N^{15}N$ or $Ta_3{}^{15}N_2^-$ + $^{14}N_2$ would be the product. This scenario only could be presented when N is labeled; otherwise, N_2 activation may be hidden without being discovered. The scenarios that N atoms or N_2−ligand exchange reactions between $^{15}N_2$ and $Ta_3{}^{14}N_2$ revealed follow the Mars−van Krevelen (MVK) mechanism.[17] The highly symmetrical structure of ^{3}9 is the key to N exchange.

3.3. Crucial Properties. Density functional theory (DFT) calculations are further employed to probe the crucial properties including the electronic structures of the key complexes in Ta_3^-/N_2 and $Ta_3N_2^-/N_2$ couplings.

In Table 1, we present the natural bond orbital (NBO) charge and the energy of the d donating orbital of the Ta_3^- and $Ta_3N_2^-$ clusters. The detailed evolution of the electronic structure along the reaction coordinate is shown in Figure S4. The activation of N_2 by a metal cluster is the reduction of $N_2{}^0$ into $2N^{3-}$; therefore, the stronger the electron supply ability and oxidation of metal, the stronger its ability to activate N_2. Compared with Ta_3^-, the metal oxidation state of $Ta_3N_2^-$ is increased, and its ability to donate electrons becomes weaker. Correspondingly, the activity of $Ta_3N_2^-$ is weaker than that of Ta_3^-. In addition, the orbital energy of π_b in $Ta_3N_2^-$ is also reduced, which makes it more difficult for the transfer of d electrons to the $\pi^*_{(N-N)}$ or $\sigma^*_{(N-N)}$ orbital.

Table 1. NBO Charges and Orbital Energies (Unit: eV) of the Major π Backdonation Donor Orbital (π_b) of Ta_3^- and $Ta_3N_2^-$ Clusters at the B3LYP/def2-TZVP + ECP Level

	nature charge		
clusters	Ta	Ta	π_b
Ta_3^-	−0.29	−0.42	1.25
$Ta_3N_2^-$	0.06	0.22	0.90

The binding of N_2 to the Ta_3^- or $Ta_3N_2^-$ cluster can occur in either the side-on (10 and 15) or end-on (5 and 10) configurations. IR spectra as a function of wavelength were calculated at the B3LYP/def2-TZVP + ECP level (Figure S5). This behavior is similar to that shown in $M^+-(N_2)_n$ systems.[22,23] End-on binding reproduced its favorite. The end-on binding is more strongly bound by 29 and 26 kJ mol^{-1} than the side-on binding for the triplet state for Ta_3^-/N_2 and $Ta_3N_2^-/N_2$, respectively.

In order to explore the effects of temperature and pressure on the reaction, the transition state ^{3}TS1 of the rate-determining step in the Ta_3^-/N_2 reaction was selected. Figure 3 shows the change of relative Gibbs free energy (ΔG, kJ mol^{-1}) along with temperature (K) at a pressure of 1 atm. One can see that ΔG increases linearly with the increase of temperature. However, ΔG decreases with increasing pressure at the temperature of 298 K although the change is small (Figure S6).

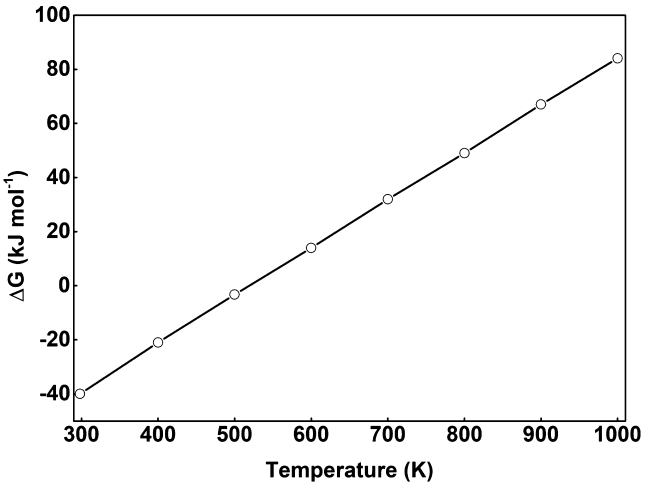

Figure 3. Change of relative Gibbs free energy (ΔG, kJ mol^{-1}) for ^{3}TS1 with temperature (K) at a pressure of 1 atm using B3LYP/def2-TZVP + ECP.

3.4. DFT Gauging. In previous studies, it was found that the structural factor plays a minor role in the single point energy (SPE) calculations, and reaction energy prediction is quite challenging for DFT methods. SPE calculations on the structures obtained at B3LYP/def2-TZVP + ECP were performed by using 13 density functionals (Table 2),[63−77] and the def2-QZVPP + ECP basis set was used. Table 3 displays the energy differences of the two spin states and the apparent barriers as computed by the 13 methods listed in Table 2. One can see that all these methods predict that the quintet state is the ground state of Ta_3^- except for M11 and most of the 13 methods could yield similar energy differences between the singlet or triplet and quintet states. Most hybrid functionals give higher results, while pure functionals give lower ones. In general, the apparent barriers increase with the increasing amount of Hartree−Fock (HF)-exchange. The highest value is twice as high as the lowest value, and some are even nearly 5 times higher.

Table 2. List of Density Functionals Used[a]

	HF-exchange (%)	References
Pure Functionals		
PBE	0	62
tHCTH	0	63
M06L	0	64
B97D	0	65
M11L	0	66
MN15L	0	67
Hybrid Functionals		
TPSSh	10	68
tHCTHhyb	15	63
B3LYP	20	69-72
X3LYP	21.8	73
BMK	42	74
BH&HLYP	50	75
wB97	100	76

[a]The color codes are as follows: (a) pure functionals (gray) and (b) hybrid functionals (yellow).

https://doi.org/10.1021/acsomega.2c02138
ACS Omega 2022, 7, 22682−22688

Table 3. Apparent Barrier ΔE (kJ mol^{-1}) for the Transition States Obtained by Various Methods at the def2-QZVPP + ECP Level

$^3Ta_3^-$		$^1Ta_3^-$		^{3}TS1		^{3}TS2	
M11L	-14	BH&HLYP	10	PBE	-156	BMK	-236
tHCTH	4	M06L	21	TPSSh	-155	TPSSh	-235
BH&HLYP	7	M15L	22	M06L	-151	M06L	-218
PBE	10	B3LYP	22	M11L	-147	PBE	-216
M06L	10	BMK	23	BMK	-141	M11L	-204
M15L	10	X3LYP	23	M15L	-127	M15L	-202
B97D	11	wB97	24	tHCTHhyb	-125	tHCTHhyb	-188
TPSSh	13	tHCTH	26	tHCTH	-113	wB97	-176
BMK	13	PBE	26	X3LYP	-103	X3LYP	-168
tHCTHhyb	13	TPSSh	27	B3LYP	-100	B3LYP	-163
B3LYP	14	tHCTHhyb	30	B97D	-83	tHCTH	-160
X3LYP	15	B97D	32	BH&HLYP	-75	BH&HLYP	-145
wB97	27	M11L	50	wB97	-72	B97D	-129
^{3}TS3		^{3}TS4		^{3}TS5		^{3}TS6	
PBE	-89	PBE	-143	BMK	-203	TPSSh	-119
M06L	-80	TPSSh	-143	TPSSh	-185	BMK	-112
TPSSh	-77	M06L	-138	M11L	-172	PBE	-105
tHCTH	-68	BMK	-138	PBE	-163	M06L	-100
M15L	-59	M15L	-127	M15L	-161	M15L	-91
tHCTHhyb	-58	M11L	-114	wB97	-158	tHCTHhyb	-75
B97D	-52	tHCTHhyb	-113	M06L	-145	M11L	-71
M11L	-52	tHCTH	-108	tHCTHhyb	-137	tHCTH	-64
X3LYP	-49	X3LYP	-93	BH&HLYP	-137	X3LYP	-57
B3LYP	-48	B3LYP	-90	X3LYP	-125	B3LYP	-54
BMK	-39	B97D	-80	B3LYP	-120	BH&HLYP	-45
BH&HLYP	-23	BH&HLYP	-75	tHCTH	-115	B97D	-40
wB97	-17	wB97	-74	B97D	-81	wB97	-39

The functional with an HF-exchange percentage of about 20% such as B3LYP gives more moderate results.

4. CONCLUSIONS

Detailed mechanisms of Ta_3^- and $Ta_3N_2^-$ clusters to activate N_2 have been explored with DFT. Thermodynamic analysis shows that Ta_3^- and $Ta_3N_2^-$ can adsorb N_2 at room temperature and cleave N≡N, and Ta_3^- has higher activity than Ta_2^+, Ta_4^+, and Ta_6^+/N_2 couplings to cleave N≡N.[16,35,46] AEAS is operated significantly on this small cluster Ta_3^-. From the functionals selected in this paper, for the time being, the density functional with an HF percentage of 20% might be used as a suitable choice for the study of such anion transition-metal systems. In addition, in the rational design of the catalyst, increasing the energy of the π-donor orbital may be a constructive strategy to reduce the effective cracking of N≡N.

Nitrogen atoms or N_2 molecules' exchange in the $Ta_3N_2^-/N_2$ scenarios are revealed following the MVK mechanism. This constitutes a rare example of complete nitrogen balance during cluster-mediated gas phase activation and is of great significance in the development of N_2 fixation as well as activation catalysts.

■ ASSOCIATED CONTENT

Supporting Information

The Supporting Information is available free of charge at https://pubs.acs.org/doi/10.1021/acsomega.2c02138.

Simplified simplified potential energy surface and key structures including selected geometric parameters for the reactions of Ta_3^- with N_2 at the B3LYP/def2-TZVP + ECP level of theory; all structures and energies calculated for the reactions of $Ta_3N_2^-$ with N_2 at the B3LYP/def2-TZVP + ECP level of theory; schematic orbital diagrams based on a frontier orbital analysis; IR spectra as a function of wavelength at the B3LYP/def2-TZVP + ECP level; and change of relative Gibbs free energy for ^{3}TS1 along the pressure at a temperature of 298 K using B3LYP/def2-TZVP + ECP(PDF)

■ AUTHOR INFORMATION

Corresponding Authors

Xiaoli Sun − *Institute of Theoretical Chemistry, Jilin University, Changchun 130023, People's Republic of China;* orcid.org/0000-0002-0509-3109; Email: Sunxiaoli@jlu.edu.cn

Xuri Huang − *Institute of Theoretical Chemistry, Jilin University, Changchun 130023, People's Republic of China;* Email: huangxr@jlu.edu.cn

Complete contact information is available at: https://pubs.acs.org/10.1021/acsomega.2c02138

Notes

The authors declare no competing financial interest.

■ ACKNOWLEDGMENTS

This research was supported by the National Natural Science Foundation of China (21903036).

■ REFERENCES

(1) Chertihin, G. V.; Andrews, L.; Bauschlicher, C. W. Reactions of Laser-Ablated Scandium Atoms with Nitrogen: Matrix Infrared Spectra and DFT Calculations for Scandium Nitrides and the Fixation of Nitrogen by Two Scandium Atoms. *J. Am. Chem. Soc.* **1998**, *120*, 3205−3212.

(2) Honkala, K.; Hellman, A.; Remediakis, I. N.; Logadottir, A.; Carlsson, A.; Dahl, S.; Christensen, C. H.; Nørskov, J. K. Ammonia Synthesis from First-Principles Calculations. *Science* **2005**, *307*, 555.

(3) Hoffman, B. M.; Lukoyanov, D.; Yang, Z.-Y.; Dean, D. R.; Seefeldt, L. C. Mechanism of Nitrogen Fixation by Nitrogenase: The Next Stage. *Chem. Rev.* **2014**, *114*, 4041−4062.

(4) Bezdek, M. J.; Chirik, P. J. Expanding Boundaries: N_2 Cleavage and Functionalization beyond Early Transition Metals. *Angew. Chem., Int. Ed.* **2016**, *55*, 7892−7896.

(5) Schlögl, R. Catalytic synthesis of ammonia—A "never-ending story"? *Angew. Chem., Int. Ed.* **2003**, *42*, 2004−2008.

(6) Jia, H.-P.; Quadrelli, E. A. Mechanistic aspects of dinitrogen cleavage and hydrogenation to produce ammonia in catalysis and organometallic chemistry: relevance of metal hydride bonds and dihydrogen. *Chem. Soc. Rev.* **2014**, *43*, 547−564.

(7) Tanaka, H.; Nishibayashi, Y.; Yoshizawa, K. Interplay between Theory and Experiment for Ammonia Synthesis Catalyzed by Transition Metal Complexes. *Acc. Chem. Res.* **2016**, *49*, 987−995.

(8) Liu, J.-C.; Ma, X.-L.; Li, Y.; Wang, Y.-G.; Xiao, H.; Li, J. Heterogeneous Fe_3 single-cluster catalyst for ammonia synthesis via an associative mechanism. *Nat. Commun.* **2018**, *9*, 1610.

(9) Ma, X.-L.; Liu, J.-C.; Xiao, H.; Li, J. Surface Single-Cluster Catalyst for N_2-to-NH_3 Thermal Conversion. *J. Am. Chem. Soc.* **2018**, *140*, 46−49.

(10) Sellmann, D. Dinitrogen-Transition Metal Complexes: Synthesis, Properties, and Significance. *Angew. Chem., Int. Ed.* **1974**, *13*, 639−649.

(11) Bazhenova, T. A.; Shilov, A. E. Nitrogen fixation in solution. *Coord. Chem. Rev.* **1995**, *144*, 69−145.

(12) Tang, X.; Hou, Y.; Ng, C. Y.; Ruscic, B. Pulsed field-ionization photoelectron-photoion coincidence study of the process N_2+hv -> N^++N+e^-: Bond dissociation energies of N_2 and N_2^+. *J. Chem. Phys.* **2005**, *123*, 074330.

(13) Vol'Pin, M. E.; Shur, V. B. Nitrogen Fixation by Transition Metal Complexes. *Nature* **1966**, *209*, 1236.

(14) Broere, D. L. J.; Holland, P. L. Boron compounds tackle dinitrogen. *Science* **2018**, *359*, 871.
(15) Légaré, M.-A.; Bélanger-Chabot, G.; Dewhurst, R. D.; Welz, E.; Krummenacher, I.; Engels, B.; Braunschweig, H. Nitrogen fixation and reduction at boron. *Science* **2018**, *359*, 896.
(16) Geng, C.; Li, J.; Weiske, T.; Schwarz, H. Ta_2^+-mediated ammonia synthesis from N_2 and H_2 at ambient temperature. *Proc. Natl. Acad. Sci. U.S.A.* **2018**, *115*, 11680−11687.
(17) Geng, C.; Li, J.; Weiske, T.; Schwarz, H. Complete cleavage of the N≡N triple bond by Ta_2N^+ via degenerate ligand exchange at ambient temperature: A perfect catalytic cycle. *Proc. Natl. Acad. Sci. U.S.A.* **2019**, *116*, 21416.
(18) Hinton, C. S.; Citir, M.; Manard, M.; Armentrout, P.B. Collision-induced dissociation of MO^+ and MO_2^+ (M = Ta and W): Metal oxide. *Int J Mass Spectrom* **2011**, *308*, 265−274.
(19) Burford, R. J.; Fryzuk, M. D. Examining the relationship between coordination mode and reactivity of dinitrogen. *Nat. Rev. Chem.* **2017**, *1*, 0026.
(20) Forrest, S. J. K.; Schluschaß, B.; Yuzik-Klimova, E. Y.; Schneider, S. Nitrogen Fixation via Splitting into Nitrido Complexes. *Chem. Rev.* **2021**, *121*, 6522−6587.
(21) Fryzuk, M. D.; Haddad, T. S.; Mylvaganam, M.; McConville, D. H.; Rettig, S. J. End-on versus side-on bonding of dinitrogen to dinuclear early transition-metal complexes. *J. Am. Chem. Soc.* **1993**, *115*, 2782−2792.
(22) Mitchell, S. A.; Lian, L.; Rayner, D. M.; Hackett, P. A. Reaction of molybdenum clusters with molecular nitrogen. *J. Chem. Phys.* **1995**, *103*, 5539−5547.
(23) Pillai, E. D.; Jaeger, T. D.; Duncan, M. A. IR Spectroscopy and Density Functional Theory of Small $V^+(N_2)_n$ Complexes. *J. Phys. Chem. A* **2005**, *109*, 3521−3526.
(24) Pillai, E. D.; Jaeger, T. D.; Duncan, M. A. IR Spectroscopy of $Nb^+(N_2)_n$ Complexes: Coordination, Structures, and Spin States. *J. Am. Chem. Soc.* **2007**, *129*, 2297−2307.
(25) Liu, F.; Li, M.; Tan, L.; Armentrout, P. B. Guided ion beam studies of the reactions of Co_n^+ (n=1−18) with N_2: Cobalt cluster mononitride and dinitride bond energies. *J. Chem. Phys.* **2008**, *128*, 194313.
(26) Kerpal, C.; Harding, D. J.; Lyon, J. T.; Meijer, G.; Fielicke, A. N_2 Activation by Neutral Ruthenium Clusters. *J. Phys. Chem. C* **2013**, *117*, 12153−12158.
(27) Dillinger, S.; Mohrbach, J.; Hewer, J.; Gaffga, M.; Niedner-Schatteburg, G. Infrared spectroscopy of N_2 adsorption on size selected cobalt cluster cations in isolation. *Phys. Chem. Chem. Phys.* **2015**, *17*, 10358−10362.
(28) Xie, H.; Shi, L.; Xing, X.; Tang, Z. Infrared photodissociation spectroscopy of $M(N_2)_n^+$ (M = Y, La, Ce; n = 7−8) in the gas phase. *Phys. Chem. Chem. Phys.* **2016**, *18*, 4444−4450.
(29) Dillinger, S.; Klein, M. P.; Steiner, A.; McDonald, D. C.; Duncan, M. A.; Kappes, M. M.; Niedner-Schatteburg, G. Cryo IR Spectroscopy of N_2 and H_2 on Ru_8^+: The Effect of N_2 on the H-Migration. *J. Phys. Chem. Lett.* **2018**, *9*, 914−918.
(30) Hübner, O.; Himmel, H.-J. Metal Cluster Models for Heterogeneous Catalysis: A Matrix-Isolation Perspective. *Chem.—Eur. J.* **2018**, *24*, 8941−8961.
(31) Luo, Z.; Castleman, A. W., Jr.; Khanna, S. N. Reactivity of Metal Clusters. *Chem. Rev.* **2016**, *116*, 14456−14492.
(32) Himmel, H.-J.; Hübner, O.; Klopper, W.; Manceron, L. Cleavage of the N_2 Triple Bond by the Ti Dimer: A Route to Molecular Materials for Dinitrogen Activation? *Angew. Chem., Int. Ed.* **2006**, *45*, 2799−2802.
(33) Gong, Y.; Zhao; Zhou, M. Formation and Characterization of the Tetranuclear Scandium Nitride: Sc_4N_4. *J. Phys. Chem. A* **2007**, *111*, 6204−6207.
(34) Zhou, M.; Jin, X.; Gong, Y.; Li, J. Remarkable Dinitrogen Activation and Cleavage by the Gd Dimer: From Dinitrogen Complexes to Ring and Cage Nitrides. *Angew. Chem., Int. Ed.* **2007**, *46*, 2911−2914.
(35) Mafuné, F.; Tawaraya, Y.; Kudoh, S. Nitrogen Molecule Adsorption on Cationic Tantalum Clusters and Rhodium Clusters and Desorption from Their Nitride Clusters Studied by Thermal Desorption Spectrometry. *J. Phys. Chem. A* **2016**, *120*, 4089−4095.
(36) Li, Z.-Y.; Mou, L.-H.; Wei, G.-P.; Ren, Y.; Zhang, M.-Q.; Liu, Q.-Y.; He, S.-G. C−N Coupling in N_2 Fixation by the Ditantalum Carbide Cluster Anions $Ta_2C_4^-$. *Inorg. Chem.* **2019**, *58*, 4701−4705.
(37) Zhao, Y.; Cui, J.-T.; Wang, M.; Valdivielso, D. Y.; Fielicke, A.; Hu, L.-R.; Cheng, X.; Liu, Q.-Y.; Li, Z.-Y.; He, S.-G.; Ma, J.-B. Dinitrogen Fixation and Reduction by $Ta_3N_3H_{0,1}^-$ Cluster Anions at Room Temperature: Hydrogen-Assisted Enhancement of Reactivity. *J. Am. Chem. Soc.* **2019**, *141*, 12592−12600.
(38) Liu, F.; Li, M.; Tan, L.; Armentrout, P. B. Guided ion beam studies of the reactions of $Co_n(+)$ (n=1-18) with N_2: Cobalt cluster mononitride and dinitride bond energies. *J. Chem. Phys.* **2008**, *128*, 194313.
(39) Tan, L.; Liu, F.; Armentrout, P. B. Thermochemistry of the activation of N_2 on iron cluster cations: Guided ion beam studies of the reactions of $Fe_n(+)$ (n=1-19) with N_2. *J. Chem. Phys.* **2006**, *124*, 084302.
(40) Shima, T.; Hu, S.; Luo, G.; Kang, X.; Luo, Y.; Hou, Z. Dinitrogen Cleavage and Hydrogenation by a Trinuclear Titanium Polyhydride Complex. *Science* **2013**, *340*, 1549−1552.
(41) Teng, Y.-L.; Xu, Q. Matrix isolation infrared spectroscopic studies and density functional theory calculations of the MNN, (MN)(2) (M = Y and La), and Y3NN molecules. *J. Phys. Chem. A* **2008**, *112*, 3607−3613.
(42) Laplaza, C. E.; Cummins, C. C. Dinitrogen Cleavage by a 3-coordinate Molubdenum(III) Complex. *Science* **1995**, *268*, 861−863.
(43) Studt, F.; MacKay, B. A.; Fryzuk, M. D.; Tuczek, F. Spectroscopic Properties and Quantum Chemistry-Based Normal Coordinate Analysis (QCB-NCA) of a Dinuclear Tantalum Complex Exhibiting the Novel Side-On End-On Bridging Geometry of N_2: Correlations to Electronic Structure and Reactivity. *J. Am. Chem. Soc.* **2004**, *126*, 280−290.
(44) Kumar Yadav, M.; Mookerjee, A. Nitrogen absorption and dissociation on small Tantalum clusters. *Phys. B* **2010**, *405*, 3940−3942.
(45) Roy, D.; Navarro-Vazquez, A.; Schleyer, P. v. R. Modeling Dinitrogen Activation by Lithium: A Mechanistic Investigation of the Cleavage of N_2 by Stepwise Insertion into Small Lithium Clusters. *J. Am. Chem. Soc.* **2009**, *131*, 13045−13053.
(46) Fries, D. V.; Klein, M. P.; Steiner, A.; Prosenc, M. H.; Niedner-Schatteburg, G. Observation and mechanism of cryo N_2 cleavage by a tantalum cluster. *Phys. Chem. Chem. Phys.* **2021**, *23*, 11345−11354.
(47) Wang, Y.; Sun, X.; Zhang, J.; Li, J. A Theoretical Study on Methane C−H Bond Activation by Bare $[FeO]^{+/0/-}$. *J. Phys. Chem. A* **2017**, *121*, 3501−3514.
(48) Sun, Y.; Sun, X.; Huang, X. Reaction of CO_2 with Atomic Transition Metal $M^{+/0/-}$ Ions: A Theoretical Study. *J. Phys. Chem. A* **2018**, *122*, 5848−5860.
(49) Fryzuk, M. D. Side-on End-on Bound Dinitrogen: An Activated Bonding Mode That Facilitates Functionalizing Molecular Nitrogen. *Acc. Chem. Res.* **2009**, *42*, 127−133.
(50) Li, Z.-Y.; Li, Y.; Mou, L.-H.; Chen, J.-J.; Liu, Q.-Y.; He, S.-G.; Chen, H. A Facile N≡N Bond Cleavage by the Trinuclear Metal Center in Vanadium Carbide Cluster Anions V3C4$^-$. *J. Am. Chem. Soc.* **2020**, *142*, 10747−10754.
(51) Mou, L.-H.; Liu, Q.-Y.; Zhang, T.; Li, Z.-Y.; He, S.-G. Reactivity of Tantalum Carbide Cluster Anions TaC_n^- (n = 1−4) with Dinitrogen. *J. Phys. Chem. A* **2018**, *122*, 3489−3495.
(52) Mou, L.-H.; Li, Y.; Li, Z.-Y.; Liu, Q.-Y.; Ren, Y.; Chen, H.; He, S.-G. Dinitrogen Activation and Functionalization by Heteronuclear Metal Cluster Anions $FeV_2C_2^-$ at Room Temperature. *J. Phys. Chem. Lett.* **2020**, *11*, 9990−9994.
(53) Mou, L.-H.; Li, Z.-Y.; Liu, Q.-Y.; He, S.-G. Size-Dependent Association of Cobalt Deuteride Cluster Anions $Co_3D_n^-$ (n = 0−4) with Dinitrogen. *J. Am. Soc. Mass Spectrom.* **2019**, *30*, 1956−1963.
(54) Frisch, M. J.; Trucks, G. W.; Schlegel, H. B.; Scuseria, G. E.; Robb, M. A.; Cheeseman, J. R.; Scalmani, G.; Barone, V.; Mennucci, B.; Petersson, G. A.; Nakatsuji, H.; Caricato, M.; Li, X.; Hratchian, H. P.;

https://doi.org/10.1021/acsomega.2c02138
ACS Omega 2022, 7, 22682−22688

Izmaylov, A. F.; Bloino, J.; Zheng, G.; Sonnenberg, J. L.; Hada, M.; Ehara, M.; Toyota, K.; Fukuda, R.; Hasegawa, J.; Ishida, M.; Nakajima, T.; Honda, Y.; Kitao, O.; Nakai, H.; Vreven, T.; Montgomery, J. A.; Peralta, J. E.; Ogliaro, F.; Bearpark, M.; Heyd, J. J.; Brothers, E.; Kudin, K. N.; Staroverov, V. N.; Keith, T.; Kobayashi, R.; Normand, J.; Raghavachari, K.; Rendell, A.; Burant, J. C.; Iyengar, S. S.; Tomasi, J.; Cossi, M.; Rega, N.; Millam, J. M.; Klene, M.; Knox, J. E.; Cross, J. B.; Bakken, V.; Adamo, C.; Jaramillo, J.; Gomperts, R.; Stratmann, R. E.; Yazyev, O.; Austin, A. J.; Cammi, R.; Pomelli, C.; Ochterski, J. W.; Martin, R. L.; Morokuma, K.; Zakrzewski, V. G.; Voth, G. A.; Salvador, P.; Dannenberg, J. J.; Dapprich, S.; Daniels, A. D.; Farkas, O.; Foresman, J. B.; Ortiz, J. V.; Cioslowski, J.; Fox, D. J. *Gaussian 09*, Revision D.01; Gaussian, Inc.: Wallingford CT, 2013.

(55) Li, J.-L.; Mata, R. A.; Ryde, U. Large Density-Functional and Basis-Set Effects for the DMSO Reductase Catalyzed Oxo-Transfer Reaction. *J. Chem. Theory Comput.* **2013**, *9*, 1799−1807.

(56) Sun, X.; Sun, X.; Geng, C.; Zhao, H.; Li, J. Benchmark Study on Methanol C−H and O−H Bond Activation by Bare $[Fe^{IV}O]^{2+}$. *J. Phys. Chem. A* **2014**, *118*, 7146−7158.

(57) van Severen, M.-C.; Andrejić, M.; Li, J.; Starke, K.; Mata, R. A.; Nordlander, E.; Ryde, U. A quantum-mechanical study of the reaction mechanism of sulfite oxidase. *J. Biol. Inorg Chem.* **2014**, *19*, 1165−1179.

(58) Fukui, K. Formulation of the reaction coordinate. *J. Phys. Chem.* **1970**, *74*, 4161−4163.

(59) Fukui, K. The path of chemical reactions—the IRC approach. *Acc. Chem. Res.* **1981**, *14*, 363−368.

(60) Truhlar, D. G.; Gordon, M. S. From Force Fields to Dynamics: Classical and Quantal Paths. *Science* **1990**, *249*, 491−498.

(61) Gonzalez, C.; Schlegel, H. B. Reaction path following in mass-weighted internal coordinates. *J. Phys. Chem.* **1990**, *94*, 5523−5527.

(62) Zhang, J.; Dolg, M. ABCluster: the artificial bee colony algorithm for cluster global optimization. *Phys. Chem. Chem. Phys.* **2015**, *17*, 24173−24181.

(63) Perdew, J. P.; Burke, K.; Ernzerhof, M. Generalized gradient approximation made simple. *Phys. Rev. Lett.* **1996**, *77*, 3865−3868.

(64) Boese, A. D.; Handy, N. C. New exchange-correlation density functionals: The role of the kinetic-energy density. *J. Chem. Phys.* **2002**, *116*, 9559−9569.

(65) Zhao, Y.; Truhlar, D. G. A new local density functional for main-group thermochemistry, transition metal bonding, thermochemical kinetics, and noncovalent interactions. *J. Chem. Phys.* **2006**, *125*, 194101.

(66) Grimme, S. Semiempirical GGA-type density functional constructed with a long-range dispersion correction. *J. Comput. Chem.* **2006**, *27*, 1787−1799.

(67) Peverati, R.; Truhlar, D. G. M11-L: A Local Density Functional That Provides Improved Accuracy for Electronic Structure Calculations in Chemistry and Physics. *J. Phys. Chem. Lett.* **2012**, *3*, 117−124.

(68) Yu, H. S.; He, X.; Truhlar, D. G. MN15-L: A New Local Exchange-Correlation Functional for Kohn−Sham Density Functional Theory with Broad Accuracy for Atoms, Molecules, and Solids. *J. Chem. Theory Comput.* **2016**, *12*, 1280−1293.

(69) Staroverov, V. N.; Scuseria, G. E.; Tao, J.; Perdew, J. P. Comparative assessment of a new nonempirical density functional: Molecules and hydrogen-bonded complexes. *J. Chem. Phys.* **2003**, *119*, 12129−12137.

(70) Becke, A. D. Density-functional exchange-energy approximation with correct asymptotic behavior. *Phys. Rev. A: At., Mol., Opt. Phys.* **1988**, *38*, 3098−3100.

(71) Lee, C.; Yang, W.; Parr, R. G. Development of the Colle-Salvetti correlation-energy formula into a functional of the electron density. *Phys. Rev. B: Condens. Matter Mater. Phys.* **1988**, *37*, 785−789.

(72) Becke, A. D. Density-functional thermochemistry. III. The role of exact exchange. *J. Chem. Phys.* **1993**, *98*, 5648−5652.

(73) Stephens, P. J.; Devlin, F. J.; Chabalowski, C. F.; Frisch, M. J. Ab Initio Calculation of Vibrational Absorption and Circular Dichroism Spectra Using Density Functional Force Fields. *J. Phys. Chem.* **1994**, *98*, 11623−11627.

(74) Xu, X.; Goddard, W. A., III From The Cover: The X3LYP extended density functional for accurate descriptions of nonbond interactions, spin states, and thermochemical properties. *Proc. Natl. Acad. Sci. U.S.A.* **2004**, *101*, 2673−2677.

(75) Boese, A. D.; Martin, J. M. L. Development of density functionals for thermochemical kinetics. *J. Chem. Phys.* **2004**, *121*, 3405−3416.

(76) Becke, A. D. A new mixing of Hartree−Fock and local density-functional theories. *J. Chem. Phys.* **1993**, *98*, 1372−1377.

(77) Chai, J.-D.; Head-Gordon, M. Systematic optimization of long-range corrected hybrid density functionals. *J. Chem. Phys.* **2008**, *128*, 084106.

https://doi.org/10.1021/acsomega.2c02138
ACS Omega 2022, 7, 22682−22688